

A dynamic cellular vertex model of growing epithelial tissues

Shao-Zhen Lin¹ · Bo Li¹ · Xi-Qiao Feng¹

Received: 20 December 2016 / Revised: 12 February 2017 / Accepted: 15 February 2017 / Published online: 10 March 2017
© The Chinese Society of Theoretical and Applied Mechanics; Institute of Mechanics, Chinese Academy of Sciences and Springer-Verlag Berlin Heidelberg 2017

Abstract Intercellular interactions play a significant role in a wide range of biological functions and processes at both the cellular and tissue scales, for example, embryogenesis, organogenesis, and cancer invasion. In this paper, a dynamic cellular vertex model is presented to study the morphomechanics of a growing epithelial monolayer. The regulating role of stresses in soft tissue growth is revealed. It is found that the cells originating from the same parent cell in the monolayer can orchestrate into clustering patterns as the tissue grows. Collective cell migration exhibits a feature of spatial correlation across multiple cells. Dynamic intercellular interactions can engender a variety of distinct tissue behaviors in a social context. Uniform cell proliferation may render high and heterogeneous residual compressive stresses, while stress-regulated proliferation can effectively release the stresses, reducing the stress heterogeneity in the tissue. The results highlight the critical role of mechanical factors in the growth and morphogenesis of epithelial tissues and help understand the development and invasion of epithelial tumors.

Keywords Soft tissue · Cellular vertex model · Cell · Morphogenesis

1 Introduction

Epithelium is ubiquitous on both the interior and exterior surfaces of organs, providing a number of significant functions, e.g., transmission, secretion, absorption, structural support, and protection [1]. Epithelial morphogenesis is critical in such biological processes as embryogenesis [2], organogenesis [3], tumorigenesis [4], and wound healing [5]. Epithelial cells are tightly connected to each other through intercellular junctions (Fig. 1a), which transmit intercellular forces. Therefore, epithelial morphogenesis not only integrates a diversity of physiological activities such as cell proliferation and apoptosis but also entails various mechanical behaviors including motion, jamming, and deformation [6–11].

The dynamics of growing epithelial tissues is characterized by a complicated interplay between intercellular interactions at the cellular level and collective motions at the tissue level. During epithelial tissue growth, the density of cells increases due to proliferation. Simultaneously, some cells may lose their ability to move freely because of jamming, which may affect the macroscopic property of epithelial tissues. For example, recent studies demonstrated that a confluent cellular colony can exhibit both solid- and fluid-like mechanical behaviors under different conditions [7]. In the former case, the cells are jammed: each cell is caged by its neighbors, and there is a high energy barrier for the cell to escape from the cage. In the latter case, the cells are unjammed: a cell can readily escape from a cage even when it is occasionally caged by its neighbors. This kind of fluid-like collective behavior of cells is often observed in wound healing and cancer invasion [6]. In addition, cell proliferation within a tissue generates mechanical forces or stresses. On one hand, it has been revealed that cell proliferation-induced stresses can fluidize tissues [12] and lead to the

✉ Xi-Qiao Feng
fengxq@tsinghua.edu.cn

¹ Institute of Biomechanics and Medical Engineering, AML, Department of Engineering Mechanics, Tsinghua University, Beijing 100084, China

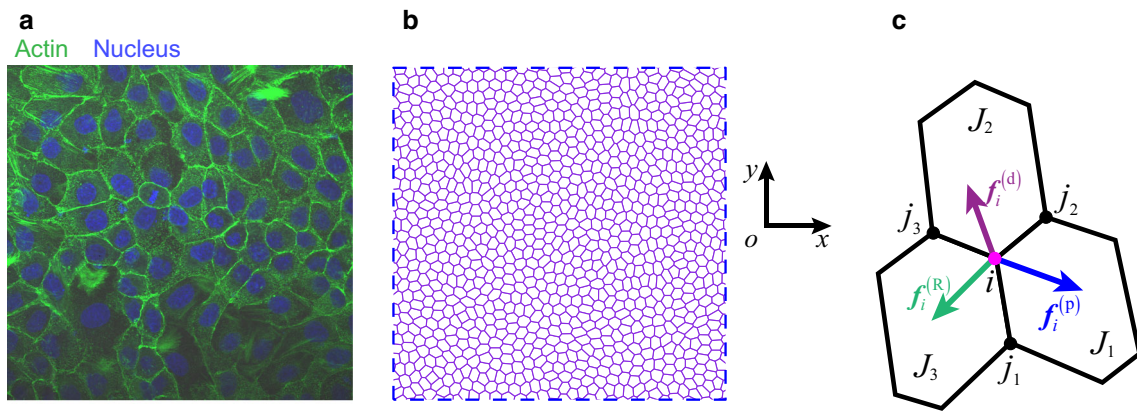


Fig. 1 **a** (Color online) Immunostaining of Madin Darby canine kidney (MDCK) cell monolayer, where the actin cytoskeleton (green) and nucleus (blue) are stained with phalloidin and DAPI, respectively. **b** Cellular vertex model in which the confluent epithelial cell monolayer is discretized into tightly connected polygons. **c** Forces acting on a vertex i , including potential force $f_i^{(p)}$, dissipative force $f_i^{(d)}$, and random force $f_i^{(R)}$

formation of swirls and clusters in the tissues [13,14]. On the other hand, the stresses accumulated in tissues can regulate cell proliferation and tissue growth. The dependence of tissue growth on internal mechanical stresses has been suggested as a possible mechanism that mediates the growth of solid tumors [15,16]. Though much attention has been devoted to epithelial growth and morphogenesis, it is still poorly understood how stress-modulated cellular behaviors influence spatiotemporal coordination at the cellular and the tissue levels.

Both continuum and discrete models have been developed to investigate epithelial morphogenesis driven by cell proliferation or tissue growth. In the continuum models, epithelium is usually treated as an elastic/viscoelastic monolayer or a fluid sheet [13,14,17], and tissue growth and induced stress are described in terms of field variables. In contrast to this class of continuum mechanics methods, the discrete description, including the particle model [12], the cellular Potts model [18], and the cellular vertex model [19–21], considers variations in individual cells. In the particle model, each cell is treated as a particle, and the interaction between two neighboring cells is characterized by a potential energy function depending on their distance. The cellular Potts model describes cells as a collection of grid points on a Cartesian mesh. The evolution of the system is governed by its total free energy, which accounts for the mechanical properties of cells, and intercellular interactions. In the present study, we adopt the cellular vertex model to describe epithelial cells, which are represented by tightly connected polygons, with vertices and edges shared by adjacent cells, as shown in Fig. 1b. Cell migration is achieved by the motion of each vertex driven by the forces acting on it (Fig. 1c).

The cellular vertex model has two main advantages. First, the cells are allowed to assume any arbitrary polygonal shape, and hence a tissue with strong anisotropic properties can be

described. Second, this method can easily incorporate the intercalation, apoptosis, and rearrangement of cells that happen in various biological processes [19]. Because of these advantages, the cellular vertex model has been extensively applied to study the ground state of epithelia [6,19,20] and cellular dynamics during epithelial morphogenesis [22–25]. This method can help shed light on many biological processes, for instance, fluid-to-solid transition driven by disease or cell motility [7,24], cancer invasion [25], and wound healing [24]. Here, we extend the vertex model to examine the morphogenesis of growing epithelial monolayers with cell proliferation. A feedback between cell proliferation and mechanical stresses is introduced into the vertex model, allowing us to explore how feedback at the cellular level tailors the macroscopic features at the tissue level.

2 Cellular vertex model

2.1 Motion equations

Here we employ a cellular vertex model to consider the growth and morphogenesis of an epithelial tissue (Fig. 1b, c). The cell dynamics is assumed to be overdamped. The motions of cells are achieved by the evolutions of the vertices. The motion of a vertex is dictated by the force balance among the potential force that stems from the potential energy of the polygonal network, the friction force induced by cell–cell and cell–substrate relative motions, and the random force due to system noises.

The potential energy in the system under study, U , characterizes cell contractility, cell area elasticity, and interfacial energy. It is expressed as [19–21]

$$U = \sum_J \frac{1}{2} K_c L_J^2 + \sum_J \frac{1}{2} K_a (A_J - A_{0J})^2 + \sum_{\langle i,j \rangle} \Lambda_{ij}, \quad (1)$$

where K_c , K_a , and Λ denote the cell contraction modulus, cell area elastic stiffness, and interfacial tension, respectively; L_J and A_J represent the perimeter and area of cell J , respectively; A_{0J} is its preferred area, which can be different for different cells, e.g., growing and nongrowing cells; l_{ij} is the length of intercellular interface ij connecting vertices i and j . It should be noted that the interfacial tension Λ relies on the competition between the cortical tension and the intercellular adhesion, and thus it can be either positive or negative [26]. In Eq. (1), the first term accounts for the cell contractility arising from the actomyosin ring beneath the plasma membrane, and the second and third terms refer to the cell elasticity and intercellular interfacial energy, respectively.

The potential force acting on vertex i can be derived as

$$f_i^{(p)} = -\nabla_i U, \tag{2}$$

where $\nabla_i = \partial/\partial r_i$ denotes the spatial gradient with respect to the position of vertex i , r_i .

Substituting Eq. (1) into Eq. (2) we obtain

$$f_i^{(p)} = - \sum_{J \in C_i} K_c L_J \left(\frac{r_i - r_{j_1}}{|r_i - r_{j_1}|} + \frac{r_i - r_{j_2}}{|r_i - r_{j_2}|} \right) - \sum_{J \in C_i} \frac{1}{2} K_a (A_J - A_{0J}) [k \times (r_{j_2} - r_{j_1})] - \sum_{j \in V_i} \Lambda \frac{r_i - r_j}{|r_i - r_j|}, \tag{3}$$

where k denotes the unit vector normal to the cell monolayer. The summation $\sum_{J \in C_i}$ computes over all neighboring cells C_i of vertex i , and j_1 and j_2 are the neighboring vertices of vertex i in cell J , as shown in Fig. 1c, while the summation $\sum_{j \in V_i}$ is made over all neighboring vertices V_i of vertex i .

The mechanical equilibrium of a vertex satisfies the balance among the potential force $f_i^{(p)}$, the dissipative force $f_i^{(d)} = -\eta dr_i/dt$, with η being the friction coefficient, and the random force $f_i^{(R)}$ accounting for system noises, as shown in Fig. 1c. Accordingly, the motion of vertex i satisfies the following Langevin equation:

$$\eta \frac{dr_i}{dt} = f_i^{(p)} + f_i^{(R)}. \tag{4}$$

The random force is taken as the Gaussian white noise [27],

$$f_i^{(R)} = \sigma_R \xi_i, \tag{5}$$

where σ_R is the intensity of the noise, and ξ_i is the unit-variance Gaussian white noise acting at vertex i satisfying

$$\langle \xi_i \rangle = \mathbf{0}, \langle \xi_{i\alpha}(t) \xi_{j\beta}(t') \rangle = \delta_{ij} \delta_{\alpha\beta} \delta(t - t'), \tag{6}$$

where $\xi_{i\alpha}$ is the α -component of ξ_i , and $\delta(t)$ and δ_{ij} are the Dirac and Kronecker delta functions, respectively. Note that the motions of epithelial cells are often affected by the interactions (e.g., shear forces) between cells and substratum. In the present study, we focus on the effects of stress regulation on epithelial growth, and, for simplicity, the cell–substratum interaction is taken into account in the friction force in Eq. (4).

2.2 Normalization scheme

Define the following dimensionless parameters:

$$\begin{aligned} \tilde{r}_i &= \frac{r_i}{\sqrt{A_0}}, \quad L_0 = \sqrt{A_0}, \quad \tilde{t} = \frac{t}{\tau_0} = \frac{\Lambda_r t}{\eta \sqrt{A_0}}, \quad \tau_0 = \frac{\eta \sqrt{A_0}}{\Lambda_r}, \\ \tilde{K}_c &= \frac{K_c \tau_0}{\eta} = \frac{K_c \sqrt{A_0}}{\Lambda_r}, \quad \tilde{K}_a = \frac{K_a A_0 \tau_0}{\eta} = \frac{K_a A_0 \sqrt{A_0}}{\Lambda_r}, \\ \tilde{\Lambda} &= \frac{\Lambda \tau_0}{\eta \sqrt{A_0}} = \frac{\Lambda}{\Lambda_r}, \quad \tilde{L}_J = \frac{L_J}{\sqrt{A_0}}, \quad \tilde{A}_J = \frac{A_J}{A_0}, \\ \tilde{A}_{0J} &= \frac{A_{0J}}{A_0}, \quad \tilde{\sigma}_R = \frac{\sigma_R \sqrt{\tau_0}}{\eta \sqrt{A_0}} = \frac{\sigma_R}{\sqrt{\tau_0} \Lambda_r}, \end{aligned} \tag{7}$$

where the length L_0 and the characteristic time τ_0 are employed to normalize Eq. (4). Λ_r is a reference intercellular tension, which is here taken as $\Lambda_r = 1$ nN according to Forgacs et al. [28]. In addition, the preferred area of a cell is set as $A_0 = 900 \mu\text{m}^2$, and the friction coefficient $\eta = 100 \text{ nN} \cdot \text{s} \cdot \mu\text{m}^{-1}$ [29]. A preliminary estimation yielded $L_0 = 30 \mu\text{m}$ and $\tau_0 = 3000 \text{ s} \approx 1 \text{ h}$. In terms of Eq. (7), the motion equation (4) is normalized as

$$\begin{aligned} \frac{d\tilde{r}_i}{d\tilde{t}} &= - \sum_{J \in C_i} \tilde{K}_c \tilde{L}_J \left(\frac{\tilde{r}_i - \tilde{r}_{j_1}}{|\tilde{r}_i - \tilde{r}_{j_1}|} + \frac{\tilde{r}_i - \tilde{r}_{j_2}}{|\tilde{r}_i - \tilde{r}_{j_2}|} \right) - \sum_{J \in C_i} \frac{1}{2} \tilde{K}_a (\tilde{A}_J - \tilde{A}_{0J}) [k \times (\tilde{r}_{j_2} - \tilde{r}_{j_1})] - \sum_{j \in V_i} \tilde{\Lambda} \frac{\tilde{r}_i - \tilde{r}_j}{|\tilde{r}_i - \tilde{r}_j|} + \tilde{\sigma}_R \tilde{\xi}_i. \end{aligned} \tag{8}$$

This normalized motion equation allows us to simulate the cellular dynamics of tissue growth. In what follows, we will drop the upper tilde for brevity. In the simulations, the following parameters are adopted unless stated otherwise: $K_a = 10.0$, $K_c = 0.2$, $\Lambda = 1.0$, and $\sigma_R = 0.01$.

2.3 Cell rearrangements

During epithelial morphogenesis, the intercalation, delamination, division, and gap closure of cells may induce cell rearrangements, which will contribute to the homeostasis and plasticity of the tissue. In the cellular vertex mode, cell rearrangements can be achieved by implementing topological transitions of the polygonal network. We consider three

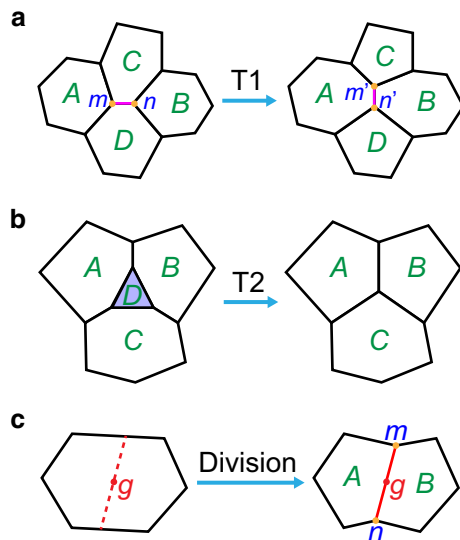


Fig. 2 Topological transitions involved in epithelial morphogenesis. **a** T1 transition induced by cell intercalation. **b** T2 transition induced by cell delamination or apoptosis. **c** Cell division. Here, *A*, *B*, *C*, and *D* refer to cells, *m*, *n*, *m'*, and *n'* represent vertices, and *g* is the geometric center of a cell

kinds of topological transitions—T1 transition, T2 transition, and cell division.

Cell intercalation induces the T1 transition. As shown in Fig. 2a, when two cells *A* and *B* that are originally separated by other cells approach each other and reach a sufficiently small distance (i.e., $|mn| < \Delta_{T1}$), they might squeeze out their neighboring cells *C* and *D* and adhere to each other, leading to the loss of interface *mn* between cells *C* and *D* and the generation of a new cell–cell interface *m'n'* between *A* and *B*. The length threshold Δ_{T1} for determining whether a T1 transition can occur should satisfy the stability criterion of the polygonal network. In our simulations, we tentatively perform a T1 transition when $|mn| < \Delta_{T1}$, but whether or not we accept this transition depends on the corresponding potential energy variation or, equivalently, the interaction forces acting on the two new vertices *m'* and *n'*. When the interaction force between the vertices and is repulsive, the tentative T1 transition is accepted.

Cell delamination or apoptosis due to overcrowding during cell proliferation may lead to a T2 transition [19], as shown in Fig. 2b. In our simulations, if a cell degenerates to a triangle (e.g., cell *D*) and its area becomes smaller than some threshold Δ_{T2} , it will be eliminated from the polygon network and its neighbors will be jointed to a point located at the geometric center of the triangle.

The division or proliferation of cells during tissue growth is illustrated in Fig. 2c. If the area of a cell becomes larger than an area threshold Δ_d , the cell will be divided into two daughter cells along the division plane passing through its geometric center (point *g* in Fig. 2c). According to Hertwig’s

cell division rule [30], the division plane should be perpendicular to the long axis of the cell. In our simulations, the long axis of a cell is defined as the straight line connecting the vertex pair that has the longest distance among all of its vertex pairs.

3 Growth of epithelial monolayer

The cellular vertex model presented in Sect. 2 is first used to study the growth of a circular epithelial monolayer. To concentrate on the role of cell proliferation, we here ignore the crawling forces induced by cell protrusions and the contractile forces generated by the supracellular actin cable within the boundary cells [31]. First, we present a scheme for simulating epithelial growth via the vertex model. Then, we investigate the free growth of a circular cell colony and will examine the supracellular pattern, the cellular motion, and the stress field in the expanding monolayer. Finally, we turn to examine the role of stress regulation on tumor growth.

3.1 Simulation scheme

In the simulations, we assume that all cells possess the potential to be activated, and activated cells will enter the mitotic cycle. Let p_{0J} denote the probability for a cell *J* to be activated per unit of time. Thus, at each time step of the simulation, the probability for an inactivated cell to enter the mitotic cycle is $p_{\Delta t}^{(J)} = 1 - (1 - p_{0J})^{\Delta t}$, where Δt is the time increment in each step. For a cell during the mitotic cycle, we increase its preferred area A_{0J} gradually to account for cell growth. Accordingly, the activated cell increases its area gradually. Once its area reaches the threshold of division, the cell will divide into two daughter cells and enter the inactivated state. The cycle period *T* of a cell is controlled in the following way: after a cell has been activated at time *t* and finally divides into two, its daughter cells are in the inactivated state and cannot enter the mitotic cycle until time $t + T$. In addition, we consider the regulation of mechanical forces on cell growth by assuming that tension promotes growth, whereas compression inhibits growth [17]. To account for the effect of mechanical stresses on cell proliferation, we assume that the probability for an inactivated cell *J* to enter the mitotic cycle per unit time, p_{0J} , is related to the stresses in the cell by

$$p_{0J} = p_0 + k_s \sigma_m^{(J)}, \tag{9}$$

where p_0 is the growth rate of a stress-free cell, k_s is the coefficient describing stress regulation of growth, and $\sigma_m^{(J)} = \frac{1}{2} (\sigma_{xx}^{(J)} + \sigma_{yy}^{(J)})$ is the mean normal stress in the cell. The stress in a cell is calculated by combining the effects of area

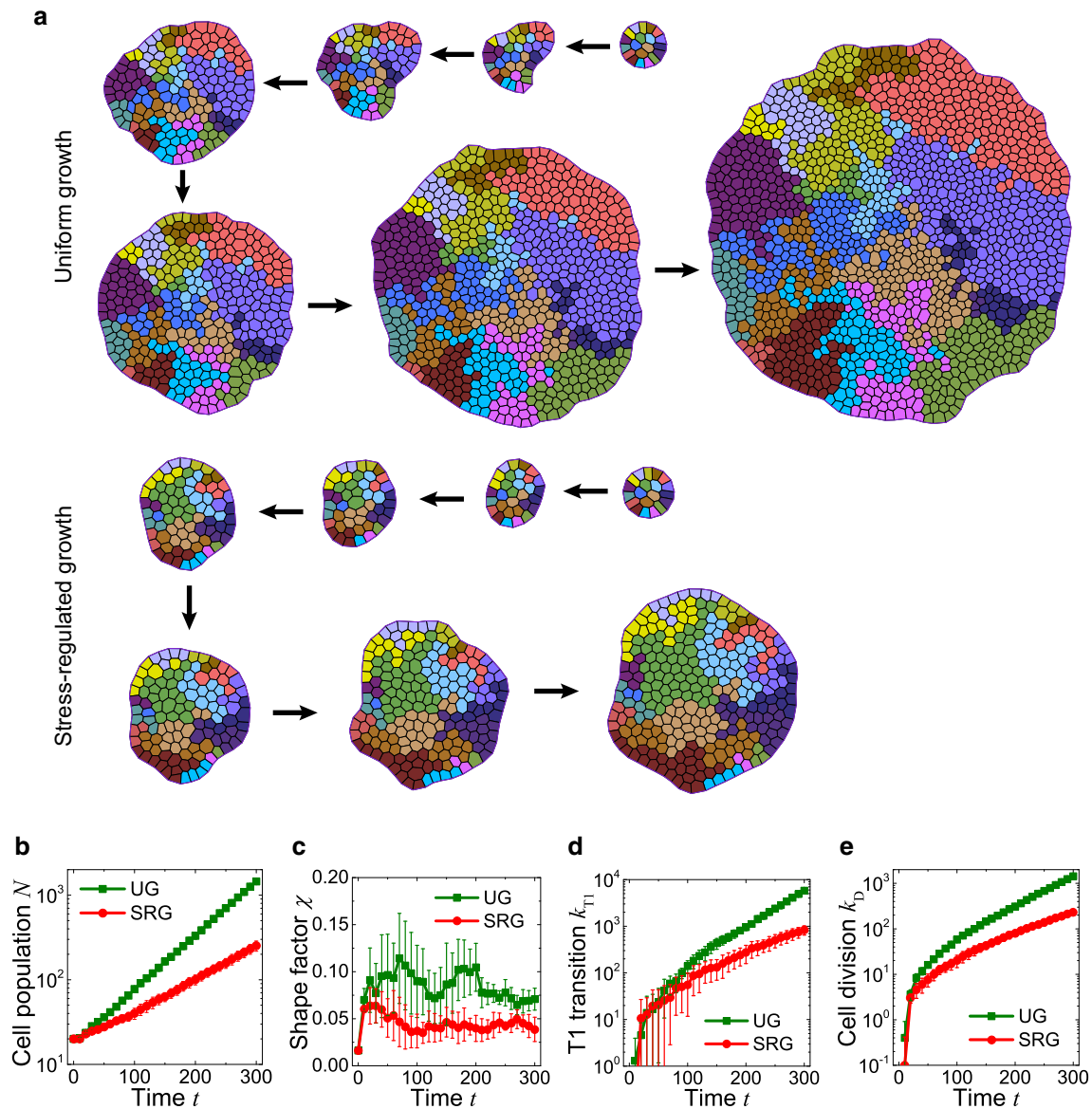


Fig. 3 (Color online) Patterns and cellular dynamics during tissue growth of a circular cell cluster containing 20 cells initially. **a** Typical morphological patterns: (*top*) UG; (*bottom*) SRG. The cells with the same color originate from the same parent cell in the initial state. For both UG and SRG, the figure sequence corresponds successively to $t = 0, 50, 100, 150, 200, 250, 300$. **b** Evolution of cell population N and **c** shape factor χ in epithelial monolayer. **d** Accumulated number of T1 transitions k_{T1} and **e** cell division k_D . In **b–e**, the data are mean \pm SD (standard deviation) ($n = 10$ simulations for each datum)

elasticity and interfacial line tension [32]. Here, we consider two cases of tissue growth. One is the stress-independent and uniform growth (UG), with $k_s = 0$, and the other is stress-regulated growth (SRG), with $k_s > 0$. The effect of stress regulation will be illustrated by comparing the two cases. Hereafter, unless noted otherwise, we use the parameters $T_c = 10.0$ and $p_0 = 0.02$. In addition, we set $k_s = 0.05$ for SRG.

3.2 Free growth

3.2.1 Cellular patterns

The morphological evolutions of a circular colony during UG and SRG are shown in Fig. 3a. To track the progenies of each cell, the cells at the initial state are plotted in different colors. As the tissue grows, the cells stemming from the same

parent cell retain the same color. It can be seen that in the cases of both UG and SRG, the cells that originate from the same cell at the initial state tend to organize into a connected cell subcluster. Different subclusters rarely diffuse or invade into each other. This dynamic behavior of cellular assembly due to tissue growth has been observed in epithelial packages [33] and could be attributed to the relatively uniform strength of cell adhesion in the tissue. For a system with a distinct difference of cell adhesion, for example, a deteriorated tumor, invasions between different subclusters may take place frequently. In addition, we find that a cell population N will obey an exponential law in the cases of both UG and SRG, as shown in Fig. 3b. The effect of stress regulation tends to lower the growth rate because the cell proliferation induces compressive stresses in the monolayer.

To quantify the shape of a cell colony, we define the shape factor $\chi = L_e^2/(4\pi A_e) - 1$, where L_e and A_e are the perimeter and area of the epithelial monolayer, respectively. The colony shape approaches a circle when χ goes to zero; it becomes narrow or rough when goes out away from zero. Our simulations show that χ is below 0.15 (Fig. 3c), indicating that the epithelium monolayer takes an approximately circular shape during growth (Fig. 3a). Figure 3d, e plots the accumulated number of T1 transitions (k_{T1}) and of cell division (k_D), respectively. It is seen that sustaining T1 transitions and cell divisions happen during the growth of the epithelial

monolayer. The accumulated numbers of these two topological transitions also follow an exponential law over time.

3.2.2 Cellular motions

We next examine cellular motions in the expanding epithelial monolayer. Figure 4a plots the trajectories of several cells during the uniform and the stress-regulated proliferation. It reveals that the collective characteristic manifests directional migration, approximately along the radial direction. To identify the migration type of the collective cells, we calculate the mean squared displacement (MSD) by

$$MSD = \left\langle |u_J(t + \Delta t) - u_J(t)|^2 \right\rangle_{J,t}, \tag{10}$$

where $u_J(t)$ is the displacement of cell J at time t , and $\langle \cdot \rangle_{J,t}$ denotes the average of all cells over time. It has been found that MSD satisfies a power law $MSD \sim (\Delta t)^\gamma$ [34]. Here, the MSD exponent γ determines the type of cell migration: $\gamma = 2$ corresponds to the ballistic or wavelike directional migration, $\gamma = 1$ the normal diffusive movement, $1 < \gamma < 2$ the superdiffusion, and $0 < \gamma < 1$ the subdiffusion [34]. It is seen that $\ln(MSD)$ increases linearly with $\ln(\Delta t)$, with the MSD exponent $\gamma = 1.831$ for UG and $\gamma = 1.708$ for SRG, indicating that the cells prefer directional migration of superdiffusion rather than subdiffusion when growth

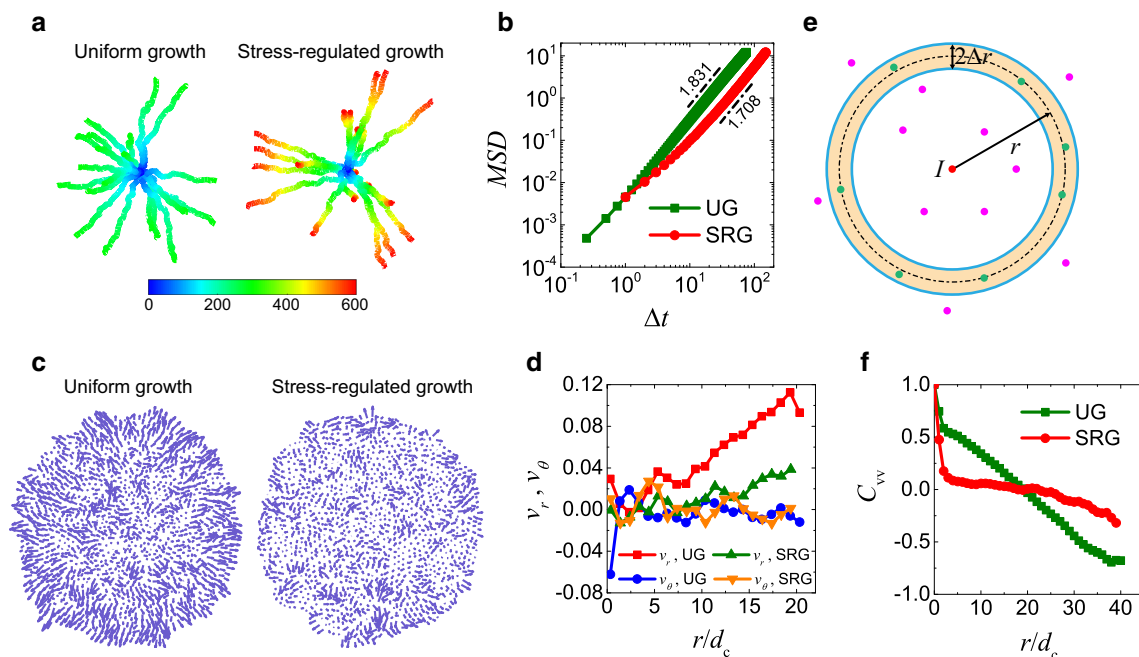


Fig. 4 (Color online) Collective cell dynamics in a freely growing epithelial monolayer. **a** Trajectories of 20 different cells. The color bar corresponds to time. **b** Mean squared displacement (MSD) of cells. **c** Typical velocity field. **d** Radial distribution of averaged radial velocity v_r and circumferential velocity v_θ corresponding to **c**, where d_c is the mean distance between neighboring cells. **e** Schematic of method of calculating spatial correlation function of velocity. The red dot is the center of cell I under consideration, the green dots are the centers of cells in the colored annulus, the pink dots are those of cells outside. **f** Spatial correlation function of velocity, $C_{vv}(r)$, corresponding to **c**

is involved (Fig. 4b). In addition, migration mode for UG is more directional than that for SRG, revealing a positive correlation between the migration mode and the rate of cell proliferation.

A typical velocity field of collective cell migration in a growing epithelial monolayer is shown in Fig. 4c. The figure illustrates that cells prefer migration along the radial direction for the cases of both UG and SRG. To quantify the directional feature of cell migrations, their velocities along the circumferential and radial directions averaged over an annulus of radius r are calculated by $v_r(r) = \left\langle v_r^{(J)} \right\rangle_{|r_J - r| < \Delta r}$ and $v_\theta(r) = \left\langle v_\theta^{(J)} \right\rangle_{|r_J - r| < \Delta r}$, respectively, where $\langle \cdot \rangle_{|r_J - r| < \Delta r}$ denotes the average over all cells in the annulus $|r_J - r| < \Delta r$, with Δr being a small half bandwidth. It is found that both the average radial velocity $v_r(r)$ and the average circumferential $v_\theta(r)$ increase with the radius r (Fig. 4d). This behavior indicates that peripheral cells migrate faster than inner ones. The circumferential velocity $v_\theta(r)$, however, fluctuates around zero and is much smaller than the radial velocity $v_r(r)$, further demonstrating the radial migration of the collective cells in the freely growing monolayer. In addition, the cell migration velocity in the case of UG is higher than that of SRG (Fig. 4d) because of the higher rate of cell proliferation in the former.

Experiments have demonstrated that collective cell migration in an epithelial monolayer often manifests a spatial long-range coordination and exhibits swirl patterns with a correlation length of several to a dozen cells [35]. Now we examine whether the tissue growth considered in the present work also renders such a velocity coordination. To quantify the local coordination of collective cells, we employ the spatial correlation function

$$C_{vv}(r) = \frac{\langle \delta v_I \cdot \delta v_J \rangle_{r, \Delta r}}{\langle \delta v_I \cdot \delta v_I \rangle_{r, \Delta r}}, \quad (11)$$

where $\delta v_I = v_I - \langle v \rangle_J$ is the velocity fluctuations of cell I obtained from its velocity v_I minus the average velocity vector. $\langle \cdot \rangle_{r, \Delta r}$ computes an average over all cell pairs (I, J) whose cell-cell distances are in a range of $r - \Delta r < |r_I - r_J| < r + \Delta r$, as shown in Fig. 4e. It is found that the collective cell migrations in an epithelial monolayer exhibit a spatial coordination of ~ 10 cells, and the correlation length in the case of UG is larger than that of SRG (Fig. 4f).

3.2.3 Stress field

We now turn to the stress field in the growing epithelial monolayer. In the cellular vertex model, the stresses in a cell, for example J , can be computed by [32]

$$\sigma_{\mu\nu}^{(J)} = S_J \delta_{\mu\nu} + \frac{1}{2A_J} \sum_{(i,j) \in E_J} T_{ij} \frac{l_{ij}^\mu l_{ij}^\nu}{l_{ij}}, \quad (12)$$

where μ and ν refer to the coordinate indices x and y , and $\delta_{\mu\nu}$ is the Kronecker delta. l_{ij}^x and l_{ij}^y represent the projection components of edge ij on the x - and y -axes, respectively. $S_J = K_a(A_J - A_0)$ denotes the stress arising from area variation, and $T_{ij} = \Lambda + K_c(L_I + L_J)$ is the tension along edge ij shared by cells I and J . The summation $\sum_{(i,j) \in E_J}$ computes over all edges E_J of cell J .

For the cases of UG and SRG, the calculation results for the stress fields in the epithelial monolayer are given in Fig. 5. Obviously, compressive stresses emerge in the monolayer as it grows. Figure 5a plots the stress fields of the radial normal stress σ_r , the circumferential normal stress σ_θ , and the mean normal stress σ_m . It is seen that the stresses are compressive almost everywhere in the monolayer. In the case of UG, the stress fields exhibit a distinct heterogeneity, while in the case of SRG the stress fields are quite homogeneous and much smaller in magnitude than those of UG. In addition, the stress fields are approximately axisymmetric. We calculate the stresses averaged over an annulus of radius r in the monolayer, that is, $\sigma_\alpha(r) = \left\langle \sigma_\alpha^{(J)} \right\rangle_{|r_J - r| < \Delta r}$, where $\alpha = r, \theta$, and m . It can be seen from Fig. 5 that $\sigma_r(r) \approx \sigma_\theta(r) \approx \sigma_m(r)$ for both the cases of UG and SRG, meaning that the cells are subjected to approximately isotropic compression. In the case of UG, $\sigma_r(r)$, $\sigma_\theta(r)$, and $\sigma_m(r)$ are all compressive and decrease with the distance r measured from the monolayer center (Fig. 5b). Thus, the cells near the center sustain larger stresses than the peripheral ones. In the case of SRG, however, the variations in $\sigma_r(r)$, $\sigma_\theta(r)$, and $\sigma_m(r)$ at distance r are much smaller, revealing an approximately homogeneous stress field. This is attributed to the effect of stress regulation on cell proliferation: compressive stresses generally suppress the rate of tissue growth and thus partly eliminate the heterogeneity of stresses in the monolayer.

Finally, we investigate the evolution of stress fields during tissue growth. Since $\sigma_r(r) \approx \sigma_\theta(r) \approx \sigma_m(r)$, only the mean normal stress σ_m will be discussed in this paragraph. Figure 6a gives the kymographs of σ_m , which characterize the crowding degree of cells in the growing cell monolayer. It is seen that in the case of UG, σ_m initially exhibits an approximately homogeneous distribution over the whole monolayer but evolves into a heterogeneous distribution gradually. The cells in the central region sustain larger compressive stresses than the peripheral ones. In the case of SRG, however, the mean normal stress σ_m remains homogeneous in the monolayer during the entire growing process. As shown in Fig. 3b, cell population N increases faster for UG than that for SRG. To compare the growth-induced stresses at the same system size, Fig. 6b shows the relation between the mean normal stress σ_m averaged over the whole tissue and the total cell

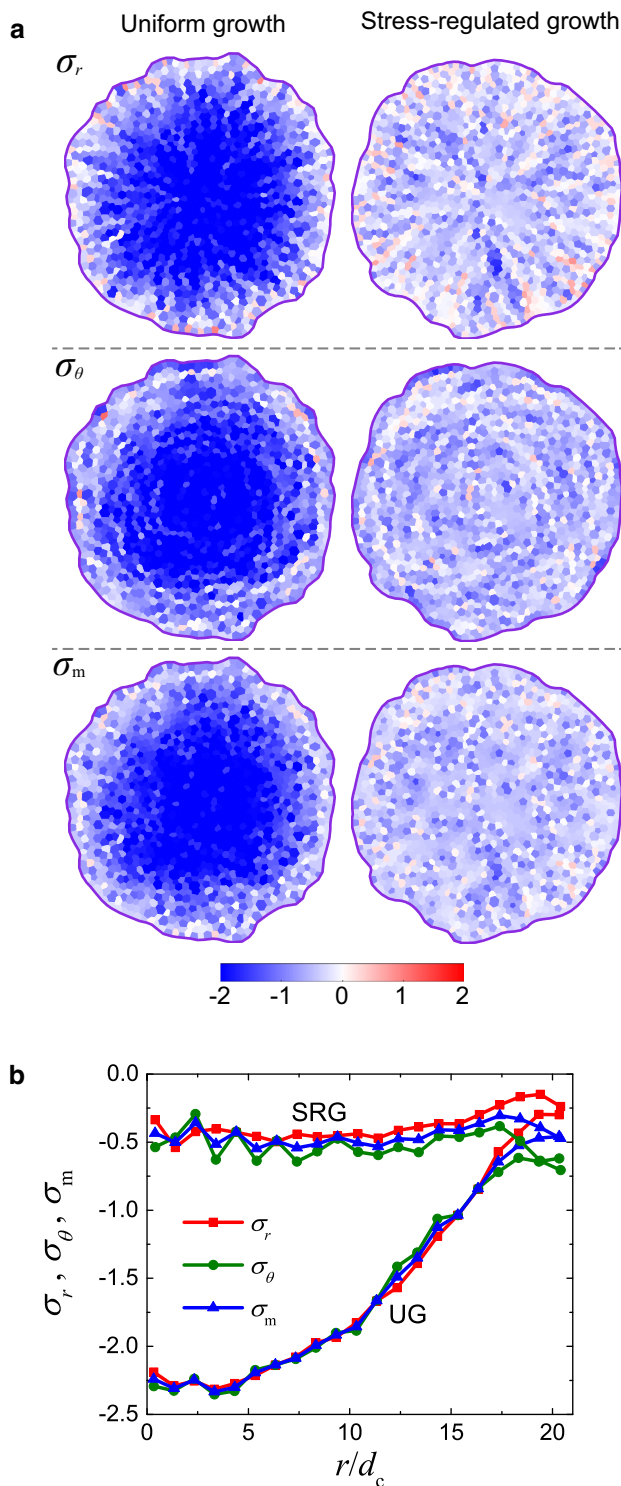


Fig. 5 (Color online) Stress field in a freely growing cell monolayer. **a** Fields of radial normal stress σ_r , circumferential normal stress σ_θ , and mean normal stress σ_m in cases of UG (left column, cell population $N = 1455$) and SRG (right column, cell population $N = 1450$). **b** Comparison of radial distributions of stresses in **a**

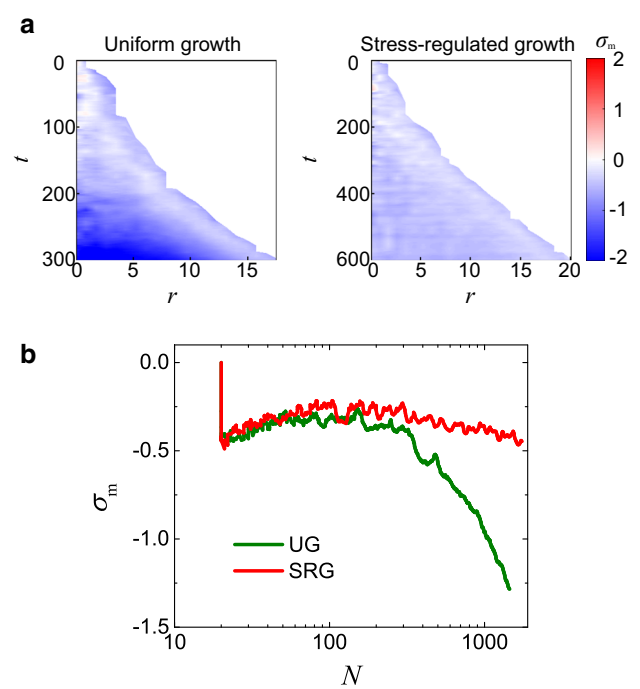


Fig. 6 (Color online) Evolution of mean normal stress during tissue growth. **a** Kymographs of mean normal stress σ_m . **b** Dependence of σ_m on cell population N

population N . In the case of UG, σ_m in the monolayer is low when the cell population is small. As the cell population increases, the compressive stress increases significantly in a logarithmic law $\sigma_m \sim \ln N$. In the case of SRG, however, the average mean normal stress σ_m remains at a relatively low level.

3.3 Confined growth

To further clarify the role of stress regulation in tumor growth, we simulate the cellular dynamics of epithelial growth in a confined space. To mimic the growth of epithelial tumors, we consider a circular cluster of cancer cells embedded in normal cells, which are confined to a circular domain, as shown in Fig. 7a. In the simulations, we take the same parameters for cancer cells and normal cells, except for the growth rate p_0 , where $p_0 = 0$ and 0.05 for normal cells and cancer cells, respectively.

The simulations show that the cancer cell cluster expands into and invades the normal cells as the tumor grows (Fig. 7a). Owing to the effect of stress regulation, the tumor grows much slower than that without stress regulation, as shown in Fig. 7b. As the tumor grows, compressive stresses are generated in the monolayer and the level of stresses may

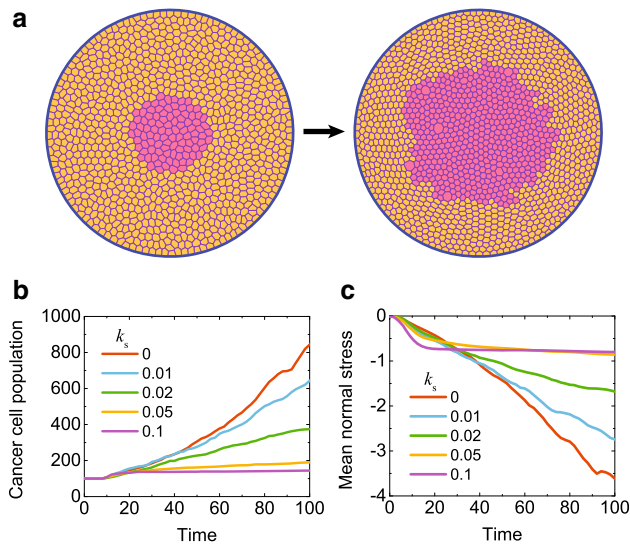


Fig. 7 (Color online) Effect of stress regulation on confined tumor growth. **a** Growth pattern of cancer cell cluster (central region in *magenta*) embedded in normal cells (periphery region in *orange*): *left*: initial state; *right*: state after tumor growth. Evolution of **b** cancer cell population and **c** mean normal stress in epithelium

approach a plateau when the stress-regulation effect is strong, for example, $k_s \geq 0.05$ (Fig. 7c). These results indicate that the stress-regulation effect modulates the growth and development of tumors undergoing confined growth: the stronger the inhibition effect of compressive stresses on cell growth, the smaller the tumor growth speed, and the lower the saturated compressive stresses.

4 Conclusions

We have developed a cellular vertex model to investigate the collective cellular dynamics in a growing epithelial monolayer with either uniform or stress-regulated cell divisions. The regulating role of stresses in tissue growth is examined. It is found that in a homogeneous monolayer with uniform intercellular adhesions, the cells can spontaneously organize into subclusters. Driven by proliferation, the cell migrations in an epithelial monolayer exhibit an anisotropic feature along the radial direction. A spatial correlation of cell migrations is observed in the growing circular monolayer. The stress-regulating mechanism of cell division tends to lower the expanding speed of the monolayer and eliminate the heterogeneity of stresses in the tissue. This work not only helps understand some biomechanical mechanisms in the growth and morphogenesis of epithelial tissues, especially the linkage between cell proliferation and mechanical stresses, but also provides clues for further investigating the morphogenesis and invasion of epithelial tumors.

Acknowledgements Supports from the National Natural Science Foundation of China (Grants 11432008, 11542005, 11672161, and 11620101001), Tsinghua University (Grant 20151080441), and the Thousand Young Talents Program of China are acknowledged.

References

- Guillot, C., Lecuit, T.: Mechanics of epithelial tissue homeostasis and morphogenesis. *Science* **340**, 1185–1189 (2013)
- Bertet, C., Sulak, L., Lecuit, T.: Myosin-dependent junction remodelling controls planar cell intercalation and axis elongation. *Nature* **429**, 667–671 (2004)
- Lubarsky, B., Krasnow, M.A.: Tube morphogenesis: making and shaping biological tubes. *Cell* **112**, 19–28 (2003)
- Balois, T., Ben Amar, M.: Morphology of melanocytic lesions in situ. *Sci. Rep.* **4**, 3622 (2014)
- Kuipers, D., Mehonic, A., Kajita, M., et al.: Epithelial repair is a two-stage process driven first by dying cells and then by their neighbours. *J. Cell Sci.* **127**, 1229–1241 (2014)
- Bi, D., Lopez, J., Schwarz, J., et al.: A density-independent rigidity transition in biological tissues. *Nat. Phys.* **11**, 1074–1079 (2015)
- Park, J.A., Atia, L., Mitchel, J.A., et al.: Collective migration and cell jamming in asthma, cancer and development. *J. Cell Sci.* **129**, 3375–3383 (2016)
- Doxzen, K., Vedula, S.R.K., Leong, M.C., et al.: Guidance of collective cell migration by substrate geometry. *Integr. Biol.* **5**, 1026–1035 (2013)
- Vedula, S.R.K., Leong, M.C., Lai, T.L., et al.: Emerging modes of collective cell migration induced by geometrical constraints. *Proc. Natl. Acad. Sci. USA* **109**, 12974–12979 (2012)
- Xu, G.K., Liu, Y., Li, B.: How do changes at the cell level affect the mechanical properties of epithelial monolayers? *Soft Matter* **11**, 8782–8788 (2015)
- Cox, B.N., Snead, M.L.: Cells as strain-cued automata. *J. Mech. Phys. Solids* **87**, 177–226 (2016)
- Ranft, J., Basan, M., Elgeti, J., et al.: Fluidization of tissues by cell division and apoptosis. *Proc. Natl. Acad. Sci. USA* **107**, 20863–20868 (2010)
- Rossen, N.S., Tarp, J.M., Mathiesen, J., et al.: Long-range ordered vorticity patterns in living tissue induced by cell division. *Nat. Commun.* **5**, 7 (2014)
- Doostmohammadi, A., Thampi, S.P., Saw, T.B., et al.: Celebrating Soft Matter's 10th Anniversary: cell division: a source of active stress in cellular monolayers. *Soft Matter* **11**, 7328–7336 (2015)
- Xue, S.L., Li, B., Feng, X.Q., et al.: Biochemomechanical poroelastic theory of avascular tumor growth. *J. Mech. Phys. Solids* **94**, 409–432 (2016)
- Stylianopoulos, T., Martin, J.D., Chauhan, V.P., et al.: Causes, consequences, and remedies for growth-induced solid stress in murine and human tumors. *Proc. Natl. Acad. Sci. USA* **109**, 15101–15108 (2012)
- Shraiman, B.I.: Mechanical feedback as a possible regulator of tissue growth. *Proc. Natl. Acad. Sci. USA* **102**, 3318–3323 (2005)
- Szabó, A., Merks, R.M.: Cellular potts modeling of tumor growth, tumor invasion, and tumor evolution. *Front. Oncol.* **3**, 87 (2013)
- Fletcher, A.G., Osterfield, M., Baker, R.E., et al.: Vertex models of epithelial morphogenesis. *Biophys. J.* **106**, 2291–2304 (2014)
- Farhadifar, R., Röper, J.C., Algouy, B., et al.: The influence of cell mechanics, cell–cell interactions, and proliferation on epithelial packing. *Curr. Biol.* **17**, 2095–2104 (2007)
- Merzouki, A., Malaspinas, O., Chopard, B.: The mechanical properties of a cell-based numerical model of epithelium. *Soft Matter* **12**, 4745–4754 (2016)

22. Vincent, J.P., Fletcher, A.G., Baena-Lopez, L.A.: Mechanisms and mechanics of cell competition in epithelia. *Nat. Rev. Mol. Cell Biol.* **14**, 581–591 (2013)
23. Loza, A.J., Koride, S., Schimizzi, G.V., et al.: Cell density and actomyosin contractility control the organization of migrating collectives within an epithelium. *Mol. Biol. Cell* **27**, 3459–3470 (2016)
24. Barton, D.L., Henkes, S., Weijer, C.J., et al.: Active vertex model for cell-resolution description of epithelial tissue mechanics. arXiv preprint, [arXiv:1612.05960](https://arxiv.org/abs/1612.05960) (2016)
25. Lin, S.Z., Li, B., Xu, G.K., et al.: Collective dynamics of cancer cells confined in a confluent monolayer of normal cells. *J. Biomech.* **52**, 140–147 (2017)
26. Manning, M.L., Foty, R.A., Steinberg, M.S., et al.: Coaction of intercellular adhesion and cortical tension specifies tissue surface tension. *Proc. Natl. Acad. Sci. USA* **107**, 12517–12522 (2010)
27. Li, B., Sun, S.X.: Coherent motions in confluent cell monolayer sheets. *Biophys. J.* **107**, 1532–1541 (2014)
28. Forgacs, G., Foty, R.A., Shafirir, Y., et al.: Viscoelastic properties of living embryonic tissues: a quantitative study. *Biophys. J.* **74**, 2227–2234 (1998)
29. Solon, J., Kaya-Copur, A., Colombelli, J., et al.: Pulsed forces timed by a ratchet-like mechanism drive directed tissue movement during dorsal closure. *Cell* **137**, 1331–1342 (2009)
30. Cadart, C., Zlotek-Zlotkiewicz, E., Le Berre, M., et al.: Exploring the function of cell shape and size during mitosis. *Dev. Cell* **29**, 159–169 (2014)
31. Anon, E., Serra-Picamal, X., Hersen, P., et al.: Cell crawling mediates collective cell migration to close undamaged epithelial gaps. *Proc. Natl. Acad. Sci. USA* **109**, 10891–10896 (2012)
32. Ishihara, S., Sugimura, K.: Bayesian inference of force dynamics during morphogenesis. *J. Theor. Biol.* **313**, 201–211 (2012)
33. Gibson, W.T., Veldhuis, J.H., Rubinstein, B., et al.: Control of the mitotic cleavage plane by local epithelial topology. *Cell* **144**, 427–438 (2011)
34. Codling, E.A., Plank, M.J., Benhamou, S.: Random walk models in biology. *J. R. Soc. Interface* **5**, 813–834 (2008)
35. Angelini, T.E., Hannezo, E., Trepat, X., et al.: Cell migration driven by cooperative substrate deformation patterns. *Phys. Rev. Lett.* **104**, 168104 (2010)